Journal of Alloys and Compounds 745 (2018) 505–512

Contents lists available at ScienceDirect

Journal of Alloys and Compounds

journal homepage: http://www.elsevier.com/locate/jalcom

Anisotropic magnetocaloric response in $AlFe_2B_2$

R. Barua [a, *], B.T. Lejeune [a], L. Ke [b], G. Hadjipanayis [c], E.M. Levin [b, f], R.W. McCallum [d], M.J. Kramer [b], L.H. Lewis [a, e, **]

[a] College of Engineering, Northeastern University, Boston, MA, USA
[b] Division of Materials Science & Engineering, Ames Laboratory, Ames, IA, USA
[c] Department of Physics and Astronomy, University of Delaware, Newark, DE 19716, USA
[d] McCallum Consulting LLC, Santa Fe, NM, USA
[e] Mechanical Engineering, Northeastern University, Boston, MA, USA
[f] Department of Physics and Astronomy, Iowa State University, Ames, IA, USA

ARTICLE INFO

Article history:
Received 5 November 2017
Received in revised form
7 February 2018
Accepted 15 February 2018
Available online 19 February 2018

ABSTRACT

Experimental investigations of the magnetocaloric response of the intermetallic layered $AlFe_2B_2$ compound along the principle axes of the orthorhombic cell were carried out using aligned plate-like crystallites with an anisotropic [101] growth habit. Results were confirmed to be consistent with density functional theory calculations. Field-dependent magnetization data confirm that the *a*-axis is the easy direction of magnetization within the (*ac*) plane. The magnetocrystalline anisotropy energy required to rotate the spin quantization vector from the *c*-to the *a*-axis direction is determined as K~0.9 MJ/m^3 at 50 K. Magnetic entropy change curves measured near the Curie transition temperature of 285 K reveal a large rotating magnetic entropy change of 1.3 J kg^{-1}K^{-1} at $\mu_0 H_{app} = 2$ T, consistent with large differences in magnetic entropy change ΔS_{mag} measured along the *a*- and *c*-axes. Overall, this study provides insight of both fundamental and applied relevance concerning pathways for maximizing the magnetocaloric potential of $AlFe_2B_2$ for thermal management applications.

1. Introduction

The magnetocaloric effect (MCE) forms the basis of two sustainable energy-related emerging technologies: (a) magnetic refrigeration - an environmentally friendly alternative to conventional vapor-compression cooling; and (b) magnetocaloric energy conversion - a thermal energy harvesting technology with an estimated energy efficiency of 30–60% of that of an ideal Carnot cycle [1,2]. By definition, the MCE describes the adiabatic temperature change (ΔT_{ad}) of a magnetic material upon application and subsequent removal of a magnetic field [1]. This effect is enhanced in the vicinity of a magnetic phase transition and is usually highly amplified in systems with strong lattice-magnetic spin coupling [1]. The magnitude of ΔT_{ad} may be estimated from temperature-dependent isothermal magnetic entropy change curves (ΔS_{mag} *vs. T* plots) constructed from thermomagnetic *M(H,T)* data measured through the coupled magnetostructural phase transition, employing Maxwell's Relations [1]. Contemplated magnetocaloric materials (MCMs) for industrially-relevant room temperature operation include the rare earth metal gadolinium (Gd) with the hexagonal structure, exhibiting room-temperature ΔS_{mag} and ΔT_{ad} values of 6–10 J kg^{-1}K^{-1} and 8–10 K, respectively, upon a magnetic field variation from 0 to 5 T [3]. The commercial potential of Gd is constrained due to its high cost ($485 per kilogram as of March 2017 and limited availability [3]). Other technologically important magnetocaloric compounds include the expensive intermetallic compound FeRh [4], the pnictides MnFe(P,As,Si,Ge) [5,6], the mechanically brittle Ni-Mn-In-based Heusler alloys [7,8] and the $La(FeSi)_{13}$-based hydrides that require complex synthesis and processing protocols, including hydrogen occlusion, to optimize their magnetocaloric response [9,10]. These MCMs undergo significant unit cell volume changes during the magnetocaloric cycle that can cause decrepitation, compromising the materials' mechanical robustness and chemical integrity [11]. In this work, we present the measured and computationally investigated thermomagnetic response along the principle symmetry axes of single crystals of the orthorhombic layered compound $AlFe_2B_2$, an

* Corresponding author.
** Corresponding author. College of Engineering, Northeastern University, Boston, MA, USA.
E-mail address: r.barua@northeastern.edu (R. Barua).

https://doi.org/10.1016/j.jallcom.2018.02.205
0925-8388/

intermetallic compound with potential to overcome limitations of existing technologically interesting MCMs. $AlFe_2B_2$ crystallizes in the orthorhombic Mn_2AlB_2-type crystal structure (space group: *Cmmm*; also referred to here as the 1-2-2 structure) with lattice parameters $a = 2.9233$ Å, $b = 11.0337$ Å and $c = 2.8703$ Å [12]. The $AlFe_2B_2$ crystal structure consists of chains of Fe-B face-sharing polyhedra oriented in the (*ac*) plane that are separated by monolayers of Al atoms located along the tetragonal *b*-axis (Fig. 1). The reduced crystallographic symmetry of the $AlFe_2B_2$ compound results in a substantial magnetocrystalline anisotropy and allows realization of an unique magnetocaloric signature along the easy and hard magnetic directions to give rise to an anisotropic magnetocaloric effect.

Only a very few studies have examined the influence of magnetic anisotropy on the magnetocaloric effect [13–15]. In 1931, Francis Bitter predicted a temperature change of the order of 0.03 K in Co due to rotation of a single crystal from the [0001] to [1010] crystallographic direction in a magnetic field of $\mu_0 H$~0.5 T [16]. In support of Bitter's hypothesis, Vonsovsky computed diverse heat capacity values along the different principle symmetry directions of cobalt [17]. A year later, Akulov and Kirensky measured the magnetocaloric effect of a Ni single crystal and demonstrated a very small (<0.1 K/T) anisotropic magnetocaloric effect arising from its low magnetocrystalline anisotropy energy [18]. Recently it has been reported that single crystals of the rare-earth metals and of rare-earth-based $RMnO_3$- and R_2MnO_5-type oxides exhibit a large anisotropic MCE associated with the strong magnetocrystalline anisotropy energy of these compounds, particularly at temperatures below 10 K [19]. Based on this concept of anisotropic magnetocaloric effect, an innovative rotary magnetic refrigerator has been proposed in which a large magnetic entropy change (ΔS_{rot}) can be realized by simply rotating the working material in a static magnetic field instead of moving it in and out of a magnet as in current active magnetic regeneration (AMR) based magnetic cooling devices [20–22]. Though it is anticipated that this budding technology may be more energy-efficient and compact than its conventional counterpart [11,20–22], no prototype for a rotating magnetic refrigerator has been constructed to date [11].

The ferromagnetic $AlFe_2B_2$ system is comprised entirely of earth-abundant, non-toxic elements with a tunable magnetic transition temperature T_c near room temperature [23–26] and is reported to exhibit ΔS_{mag} values in the range 2.1–4.4 J kg^{-1}K^{-1} at $\mu_0 H = 2$ T [23–33]; these values have been reported from polycrystalline specimens of uncertain isotropy. Neutron diffraction and Mössbauer experiments reveal that the magnetic moments in $AlFe_2B_2$ are oriented along the crystallographic *a*-axis [24,31]. With respect to magnetic cooling applications, other technologically important aspects of $AlFe_2B_2$ include anticipated ease of manufacturing [27], good chemical stability complemented with desirable mechanical robustness derived from negligible volumetric changes through the magnetocaloric cycle [28] and a favorably low heat capacity ($C_p = 115$ J-mole^{-1}K^{-1} [25]) fostering good heat transfer from the active material to the working fluid. First-principles investigations of the magnetocrystalline anisotropy energy (MAE) of $AlFe_2B_2$ report a value of K~1.37 MJ/m^3 within generalized gradient approximation (GGA) when the spin quantization vector rotates from the *c*-axis to the *a*-axis direction while the calculated anisotropy within the (*ab*)-plane was found to be almost negligible, K~0.07 MJ/m^3 [34]. The sizeable magnetocrystalline anisotropy between *c*-axis and *ab*-plane portend that a room-temperature anisotropic magnetocaloric effect exists in $AlFe_2B_2$.

To this end, experimental investigations of the magnetocaloric response of $AlFe_2B_2$ along its orthorhombic principle axes were carried out using aligned plate-like $AlFe_2B_2$ crystallites with an anisotropic growth habit along the [101] direction. Consistent with information derived from computational studies, the magnetocrystalline anisotropy energy within the *ac*-plane was determined as K~0.9 MJ/m^3 at 50 K. Magnetic entropy change curves measured near the Curie transition temperature reveal large differences in magnetic entropy change ΔS_{mag} along the *a*- and *c*-axes and appreciable rotating magnetic entropy change was found near room temperature at technologically feasible low magnetic fields ($\mu_0 H_{app}$ ranging from 1 to 2 T). These results provide insight concerning pathways for maximizing the magnetocaloric potential of $AlFe_2B_2$ for thermal management applications such as magnetic cooling and energy harvesting.

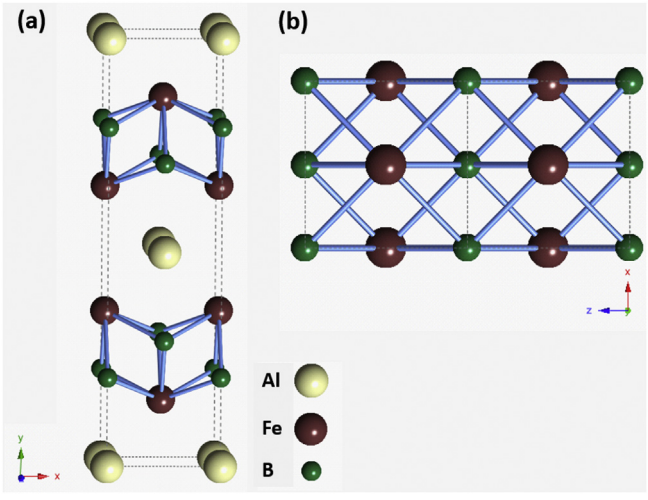

Fig. 1. Schematic representation of the orthorhombic crystal structure of $AlFe_2B_2$ from two perspectives: (a) Viewed along the *b*-axis, each unit cell consists of two formula units with Fe and B atoms forming chains of FeB polyhedra within the (*ac*) plane. Each slab is separated by a monolayer of Al atoms; (b) Top-view of the *ac*-plane indicates that the Fe_2B_2 chains form a wavy layer with Fe atoms located between parallel layers of B atoms.

2. Materials & methods

An Al-rich $AlFe_2B_2$ sample was synthesized by arc melting high-purity elemental granules (99.99% pure) of Al, Fe and B in the ratio 3:2:2, respectively. The arc-melted charge was subsequently sliced into disks (~3 mm diameter, 1 mm width) using a low-speed diamond saw and was metallographically polished to a mirror finish. Microstructural observation was carried out using optical and scanning electron microscopy (SEM, Hitachi S4800) and the chemical composition of each phase within the sample was determined using SEM energy-dispersive x-ray spectrometry (EDS). In accordance with a previous study conducted by the current authors, it was found that the as-cast samples are multiphase in character comprising of a network of elongated plate-like $AlFe_2B_2$ crystallites in an Al-rich matrix [28]. Building on this work, crystallites of $AlFe_2B_2$ were extracted from a large slice of the as-cast material by etching the sample with 50% v/v HCl at room temperature for 30 h. All subsequent characterization was performed on the samples in this above-described crystallite form.

The layered orthorhombic *Cmmm*-type crystal structure of the $AlFe_2B_2$ crystallites was confirmed by analysis of X-ray diffraction (XRD) data collected with the use of a Bruker APEX2 diffractometer equipped with a Cu-K_α radiation source ($\lambda = 1.54$ Å). Lattice parameters were determined using Rietveld refinements in the program X'Pert HighScore Plus. The atomic structure of the crystallites

was examined using high resolution transmission electron microscopy (TEM; model JEOL 2010 operated at 200 kV). TEM sample preparation was accomplished using the liquid exfoliation technique involving ultrasonication of a liquid suspension comprising of $AlFe_2B_2$ crystallites suspended in isopropyl alcohol at room temperature. Approximately 10 μL of this suspension was placed over a carbon-coated copper grid and the solvent was evaporated at room temperature. The crystallographic orientation of the $AlFe_2B_2$ crystallites, relative to the [101] fast growth direction, was determined from information obtained from the SEM micrograph and the TEM selected-area electron diffraction (SAED) pattern. Following this examination, a single $AlFe_2B_2$ crystallite (~1 mm long, ~20–30 μm wide, less than 10 μm thick) was mounted on a glass slide for magnetic characterization carried out in magnetic fields up to $\mu_0 H_{app} = 5$ T and in the temperature range $50\ K \leq T \leq 390$ K using a vibrating sample magnetometer (Quantum Design Versalab) and a superconducting quantum interference device magnetometer (Quantum Design SQUID MPMS).

The anisotropy field (H_a) in the *ac*-plane was determined using *M(H)* data measured by applying the magnetic field parallel to the crystallographic *a*- and *c*-axes. The uniaxial magnetocrystalline anisotropy constant (K_1) was estimated from formula [35]:

$$K_1 = \frac{H_a \rho M_s}{2} \tag{1}$$

Here, H_a is the anisotropy field along the hard axis, M_s is the saturation magnetization of the sample in emu/g and ρ is the density of the crystallite as determined from XRD measurements.

The magnetocaloric behavior of $AlFe_2B_2$ in the magnetic field range $0.5 < \mu_0 H_{app} < 2$ T was indirectly assessed using magnetic entropy change curves (ΔS_{mag} *vs. T*) constructed by applying Maxwell's relation to data obtained from isothermal *M*(*H*) curves measured at temperature intervals of 2.5 K in the vicinity of the Curie temperature, Eq. [2]:

$$\Delta S_{mag} = \mu_o \int_0^{H_{max}} \left(\frac{\partial M}{\partial T}\right)_H dH \tag{2}$$

Here, μ_o is the permeability of free space, $\frac{\partial M}{\partial T}$ is the temperature change of magnetization and H_{max} is the maximum applied field. The temperature sweep rate for all temperature-dependent magnetic measurements was set at 2 K/min and the magnetic transition temperature T_c was determined as the inflection point in the derivative of magnetization *M* as a function of temperature *T* at an applied field of 0.1 T. For all magnetic and indirect magnetocaloric measurements the external magnetic field was applied in the plane of the crystallite, either along the *a* or the *c*-axis of the orthorhombic crystal structure and no demagnetization corrections were applied.

The influence of magnetocrystalline anisotropy on the magnetocaloric response of the $AlFe_2B_2$ crystallites was quantified by calculating the rotational magnetocaloric effect (ΔS_{rot}) of the sample using two independent approaches. While the first method simply involves subtraction of the magnetic entropy changes obtained by applying the magnetic field along the *a*- and *c*-axes respectively ($\Delta S_{rot} = \Delta S_{a-axis} - \Delta S_{c-axis}$) [22], the second method requires determination of the anisotropy energy E_a of the sample by subtracting the area under the *M*-*H* curves measured at constant temperature for different field magnitudes that were applied parallel along the *a*- or the *c*-crystallographic axes. Subsequently, the ΔS_{rot} was also determined using the expression [20]:

$$\Delta S_{rot} = \left[\frac{\delta E_{a.H}}{\delta T} - \frac{\delta E_{a.0}}{\delta T}\right] = \frac{\delta \Delta E_a}{\delta T} \tag{3}$$

Following the procedure outlined by Fries et al. [36], the anisotropy factor (η) - a figure of merit that quantitatively describes the effect of magnetocrystalline anisotropy on the magnetocaloric effect, was determined as:

$$\eta_{anisotropy} = \frac{\Delta S_{max,\ a-axis} - \Delta S_{max,c-axis}}{\Delta S_{max,\ a-axis}} \tag{4}$$

In this formalism, $\eta_{anisotropy} = 0$ describes an isotropic material system where the magnetocrystalline anisotropy has no impact on magnetic entropy change along the principle *a*- and *c*-axis. Depending upon the magnetocrystalline anisotropy energy, $\eta_{anisotropy}$ can vary from 0 to 1.

The MAE was calculated using a standard linear muffin-tin orbital (LMTO) basis set generalized to full potentials (FP) [37]. This scheme employs generalized Hankel functions as the envelope functions. Density function theory (DFT) calculations were carried out within the generalized gradient approximation GGA (exchange correlation parametrization: Perdew, Burke, and Ernzerhof or PBE [38]) and the local density approximation LDA (exchange-correlation parametrization: Von Barth and Hedin [39]). The magnetocrystalline anisotropy energy (MAE) was calculated using the force theorem [37]. Starting from the self-consistent scalar-relativistic potential, the spin-orbit coupling was included in a subsequent one-step calculation with spin aligned along the given direction $\hat{n}$. The MAE was characterized as $K = E_c - E_a$, where E_c and E_a are the summation of occupied band energies for the magnetization oriented along the c- and *a*- axis, respectively. Both experimental and theoretical structures (from Ref. [40]) were used to calculate MAE. To compare, we also calculate the MAE within GGA by using Vienna ab initio simulation package (VASP) [41], and obtain very similar results. Complete details of the methodology of the computational calculations are provided in Ref. [35].

3. Results

Experimental results obtained from characterization of the $AlFe_2B_2$ crystallites reveal important correlations between crystal structure, magnetic properties and magnetocaloric response in this intermetallic system. In the following paragraphs, the structural and magnetic attributes of the crystallites are described first in Sections (i) and (ii), the magnetocaloric properties are reported next in Section (iii) and finally the theoretical magnetic properties of the $AlFe_2B_2$ structure as obtained using density functional theory band structure calculations are presented in Section (iv).

3.1. Structural attributes

The microstructure of the precursor $Al_3Fe_2B_2$ slab sample consists of a network of elongated $AlFe_2B_2$ crystallites in an Al-rich matrix, Fig. 2(a), in agreement with previous reports by the current authors [28]. After dissolution of the matrix phase, plate-shaped $AlFe_2B_2$ crystallites (~1–2 mm long, ~100 μm wide) consisting of very fine lamellae of submicron thickness were obtained, Fig. 2(b) and (c). The lamellae are considered to be an artifact of the acid dissolution procedure. High-resolution TEM of the etched crystallites reveals regularly spaced lattice fringes along the *c*-axis and the SAED pattern measured along the [020] zone axis indexes to a non-cubic crystal structure with *a*- and *c*-lattice parameters corresponding to 2.92 (9) Å and 2.87 (9) Å, respectively, Fig. 3.

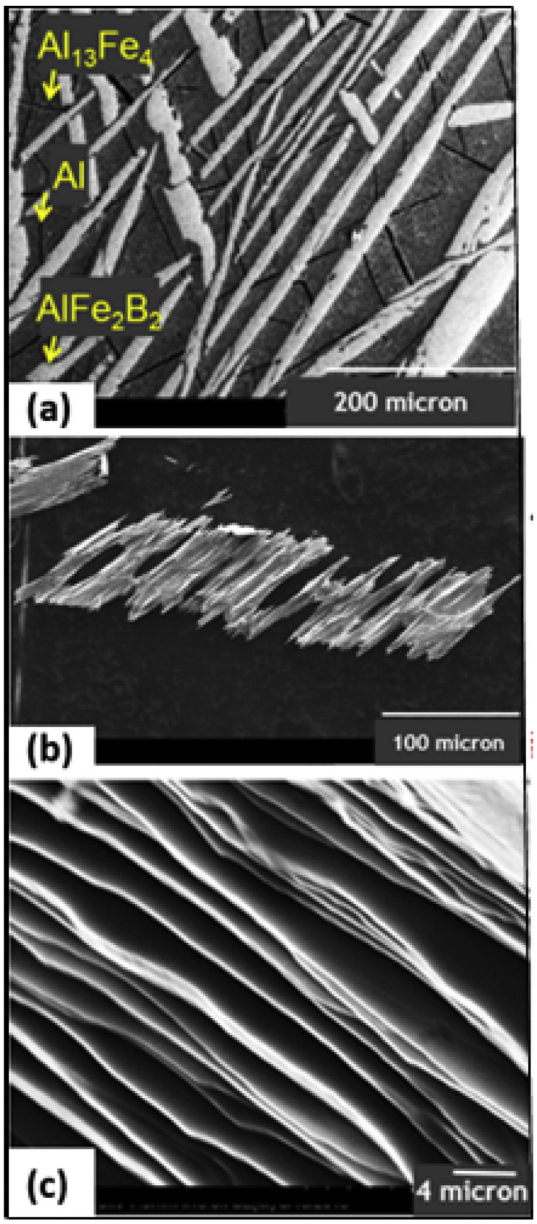

Fig. 2. a) SEM micrograph reveals that the microstructure of the precursor $Al_3Fe_2B_2$ sample consists of a network of elongated plate-like $AlFe_2B_2$ crystallites in an Al-rich matrix; (b) Plate-shaped $AlFe_2B_2$ crystallite obtained after etching the $Al_3Fe_2B_2$ ingot in dilute HCl (1:1 v/v) for 30 h; (c) Laminations of submicron thickness in the etched $AlFe_2B_2$ crystallite.

Consistent with data obtained by electron diffraction, XRD reveals that the unit cell lattice parameters of the $AlFe_2B_2$ crystallites are $a = 2.929(0)$ Å, $b = 11.034(9)$ Å and $c = 2.866(2)$, Fig. 4. The atomic coordinates and occupancies obtained from the refined structure model are listed in Table 1 and are in agreement with those reported by W. Jeitschko in 1969 [12].

3.2. Magnetic attributes

Temperature-dependent magnetization curves of a single $AlFe_2B_2$ crystallite obtained upon heating from 50 K to 400 K at applied fields $\mu_0 H_{app}$ of 0.1 T and 2 T are consistent with the existence of a ferromagnetic-to-paramagnetic Curie transition that takes place upon heating at T_c ~285 K, Fig. 5(a). The overall magnetization of the crystallite was found to be greater when the magnetic field was applied parallel to the *a*-axis than along the corresponding *c*-axis and it was observed that the difference in magnitude of the magnetization along the two in-plane orthogonal directions ($\Delta M = M_{a\text{-}axis} - M_{c\text{-}axis}$) decreases as a function of increasing magnetic field ($\Delta M = 48$ emu/g and 13 emu/g at $\mu_0 H_{app} = 0.1$ T and 2 T, respectively). Field-dependent magnetization data measured at T = 50 K indicates that the saturation magnetization (M_s) of the etched crystallite is ~78 emu/g and it is observed that the magnetic field necessary to saturate the magnetization of the sample along the *c*-axis is $\mu_0 H_a$~4 T, much larger than the value of $\mu_0 H_a$~0.1 T needed to saturate along the *a*-axis, Fig. 5(b). Following Equation [1], the magnetic anisotropy constant in the (*ac*)-plane was determined as K~0.9 ± 0.1 MJm^{-3} at T = 50 K.

3.3. Magnetocaloric attributes

The calculated magnetic entropy change curves (ΔS_{mag} *vs. T* plots, Eq. [2]) of the $AlFe_2B_2$ crystallites in the magnetic field range $\mu_0 H = 0.5$ T–2 T reveal that the maximum magnetic entropy change measured with the field applied along the *a*-axis ($\Delta S_{max,a}$) is always larger than that obtained along the orthogonal *c*-axis ($\Delta S_{max,c}$). Irrespective of the direction of applied magnetic field, the peak of the magnetic entropy curve is always observed at *T*~283 K. As an example, Fig. 5(a) shows that the magnitude of the magnetic entropy change along the *a*-axis $\Delta S_{max,a}(2\,\text{T}) = 3.6\,\text{J kg}^{-1}\text{K}^{-1}$ is ~50% greater than that measured along the *c*-axis at $\Delta S_{max,c}(2\,\text{T}) = 2.4\,\text{J kg}^{-1}\text{K}^{-1}$. Using Eq. [3], the corresponding maximum rotating magnetic entropy change at $\mu_0 H = 2$ T was calculated as $\Delta S_{rot,max} = 1.3\,\text{J kg}^{-1}\text{K}^{-1}$, Fig. 6(b). In the magnetic field range 0.5 T–2 T, $\Delta S_{rot,\,max}$ increases with increased applied magnetic field, Fig. 7(a). For reference, differences in maximum magnetic entropy change values of this compound between the *a*- and *c*-axis ($\Delta S_{max,a}$ - $\Delta S_{max,c}$) are also plotted in Fig. 7(a) and it is interesting to note that the obtained values are comparable to $\Delta S_{rot,\text{max}}$. Conversely, the field dependence of the anisotropy factor η decreases dramatically from 75% in a field change of 0.5 T–33% in a change of 2 T, as shown in Fig. 7(b).

3.4. Density functional theory band structure calculations

Table 2 summarizes the MAE values of $AlFe_2B_2$ within the *ac*-plane calculated using different approaches. Using the experimental structure, LDA gives $K = 0.82$ MJ/m^3, agreeing well with the experimental value of 0.9MJ/m^3. GGA calculations using FP-LMTO and VASP give very similar results but somewhat overestimate the MAE. Irrespective of the method used, the resultant magnetocrystalline anisotropy energy values determined using an experimental structure were found to be 10% larger than the corresponding values obtained using the theoretically optimized structure. This is likely due to the slight underestimation of lattice parameters using DFT.

4. Discussion

All experimental data derived from morphological, structural and magnetic measurements reported here indicate that the intermetallic boride $AlFe_2B_2$ exhibits an anisotropic magnetocaloric response. This feature must be considered while evaluating this compound's potential for room-temperature magnetic refrigeration technology. In subsequent paragraphs, the following aspects of the $AlFe_2B_2$ crystallites are discussed: crystallographic and microstructural attributes, magnetic response and implications of these results in the context of active magnetic regeneration (AMR) and

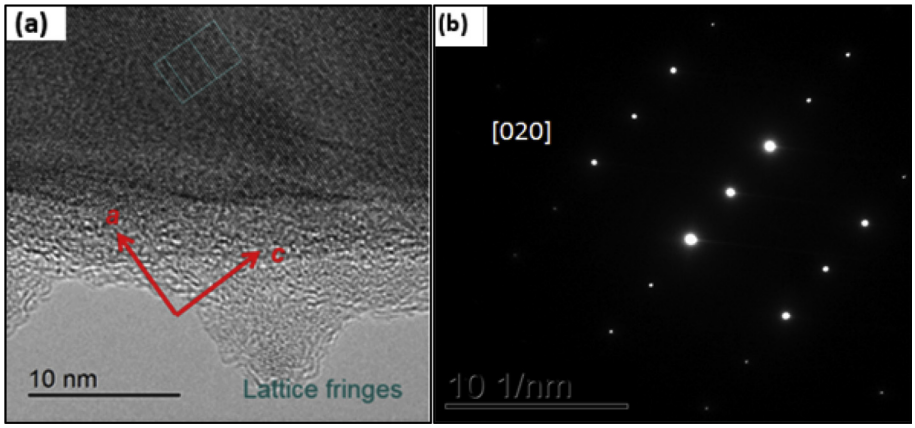

Fig. 3. X-ray diffraction pattern of a single etched $AlFe_2B_2$ crystallite reveals a *Cmmm*-type (space group: 65) orthorhombic crystal structure $a = 2.929(0)$ Å, $b = 11.034(9)$ Å and $c = 2.866(2)$.

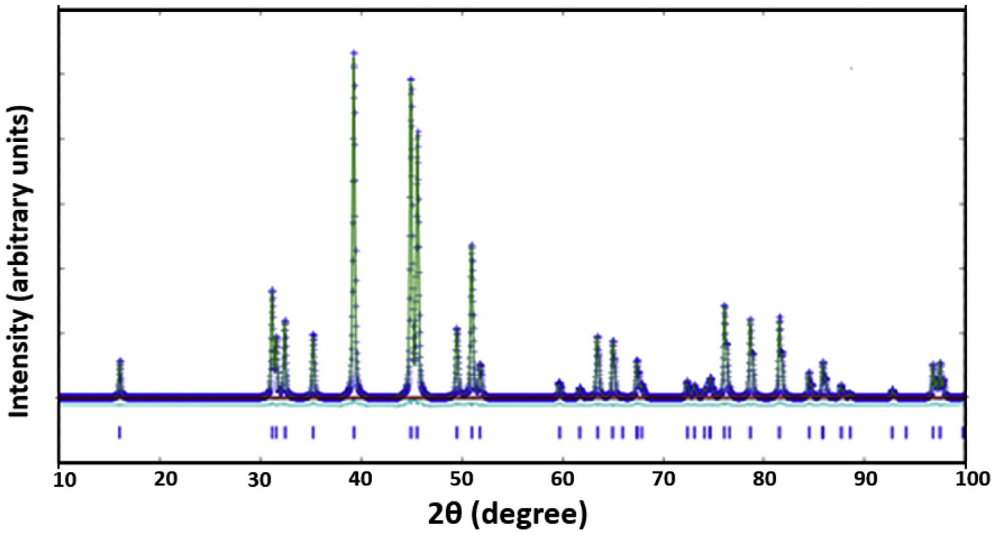

Fig. 4. (a) High-resolution TEM of the etched crystallites, reveals regularly spaced lattice fringes along the c-axis (*d-spacing* = 2.014 Å); (b) Selected-area electron diffraction (SAED) pattern taken along the [020] zone axis reveals the single crystal character of the sample. Bragg reflections index to a non-cubic crystal structure with *a* and *c* lattice parameters corresponding to 2.92 Å and 2.87 Å, respectively.

Table 1
Atomic coordinates and occupancies for $AlFe_2B_2$ at room temperature from XRD refinement.

Atom	Site	x	y	z	Occ.
Al	*2a*	0.0000	0.0000	0.0000	1
Fe	*4j*	0.0000	0.3540 (1)	0.5000	1
B	*4i*	0.0000	0.2064 (3)	0.0000	1

rotary magnetic cooling devices.

In alignment with the experimental reports of Lu and co-workers [42], SEM and TEM micrographs indicate that the etched $AlFe_2B_2$ crystallites possess an anisotropic growth habit (see Figs. 2(b) and 3). The crystal structure and the measured room-temperature lattice parameters ($a = 2.929(0)$ Å, $b = 11.034(9)$ Å and $c = 2.866(2)$) of the plate-like crystallites of $AlFe_2B_2$ are consistent with those reported in previous studies [23,28,29]. The experimentally determined magnetic properties of the crystallites are well within the range reported in the $AlFe_2B_2$ literature for this composition [24–28,30,31]. It is noted that Table 3 documents a significant spread in the reported values of the intrinsic magnetic properties M_s (1–1.32 μ_B/Fe) and T_c (280 K –325 K) for $AlFe_2B_2$. This range in the reported magnetic properties is attributed partially to chemical disorder due to non-equilibrium occupation of atomic sites within the $AlFe_2B_2$ lattice.

Magnetic data shown in Fig. 5 indicate that within the (*ac*) plane of the 1-2-2 compound, the unit cell *a*- and *c*-axes are the easy and hard direction of magnetization, respectively – an observation that is consistent with results derived from recent neutron scattering experiments [31] and computational calculations [34]. In agreement with calculated MAE values using electron FP-LMTO methods (see Table 2), the measured magnetic anisotropy energy in the *ac*-plane is K~0.9 MJ/m^3 at T = 50 K. The anisotropic magnetic properties of this structure deliver an anisotropic magnetocaloric effect. In particular, it is observed that the magnitude and shape of the magnetic entropy change curve (ΔS *vs.* T curve) is significantly altered when the applied magnetic field is directed along different crystallographic directions within the (*ac*)-plane, Fig. 6(a). At an applied magnetic field of $\mu_o H = 2$ T, the maximum magnetic entropy change in the $AlFe_2B_2$ crystallites was calculated as $\Delta S_{max,a} = 3.6\,J\,kg^{-1}K^{-1}$ and $\Delta S_{max,c} = 2.4\,J\,kg^{-1}K^{-1}$, respectively. With an exception of the ΔS_{mag} value reported by Tan et al.

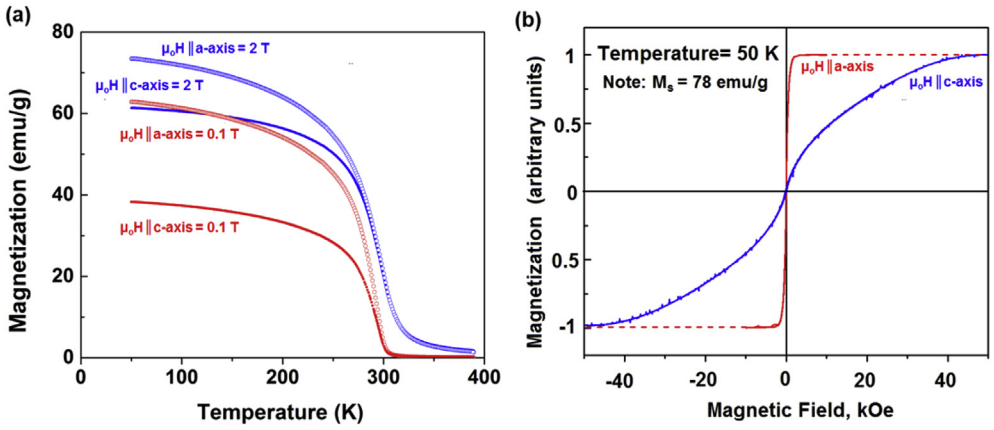

Fig. 5. Temperature-dependent magnetization curves of a single $AlFe_2B_2$ crystallite, obtained at an applied field ($\mu_0 H_{app}$) of 0.1 T and 2 T; (b) Field-dependent magnetization curves of the sample at 50 K. For all magnetic measurements, the external magnetic field was applied in the (*ac*) plane, either along the *a*- or the *c*-axis of the orthorhombic crystal structure.

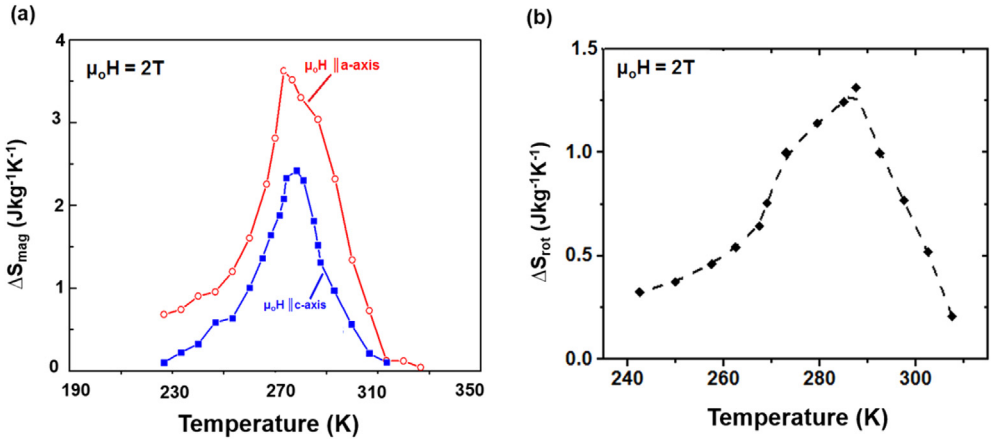

Fig. 6. (a) Magnetic entropy curves (ΔS_{mag} *vs. T* plot) and (b) Rotating magnetic entropy curves (ΔS_{rot} *vs. T* plot) of the $AlFe_2B_2$ crystallites at $\mu_0 H = 2$ T.

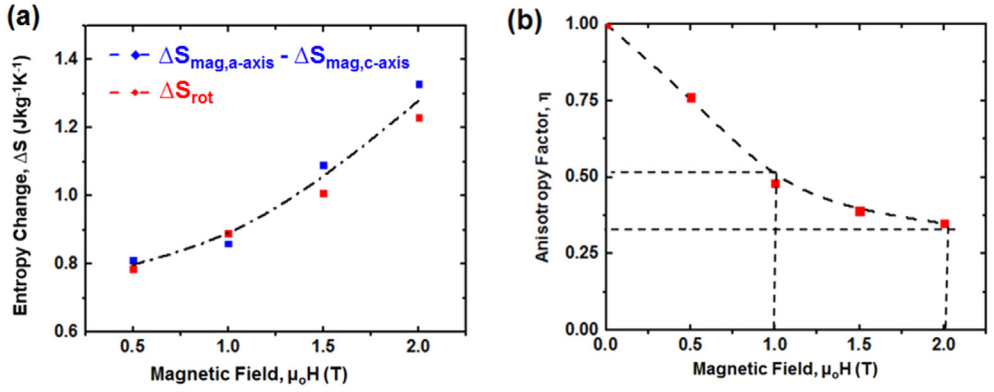

Fig. 7. (a) Magnetic field dependence of the maximum rotational magnetic entropy change ($\Delta S_{rot,\ max}$) in magnetic fields ranging from 0.5 T to 2 T. For reference, differences in entropy changes between the *a*- and *c*-axis ($\Delta S_{max,a} - \Delta S_{max,c}$) are also plotted; (b) Magnetic field dependence of the anisotropy factor (η).

(4.1 J kg^{-1}K^{-1} at $\mu_0 H = 2$ T) [25], the $\Delta S_{max,a}$ and $\Delta S_{max,c}$ of the $AlFe_2B_2$ crystallites are within the range of previously reported ΔS_{mag} values for polycrystalline $AlFe_2B_2$ compounds (see Table 3 for details). The documented spread in the entropy change ΔS_{mag} reported in Table 1 is partially attributed to averaging of the contribution of the magnetocrystalline anisotropy in these isotropic samples. In support of this conclusion, it is important to note that the magnetic entropy change values determined in this study of $\Delta S_{mag,a} = 3.6$ J kg^{-1}K^{-1} and $\Delta S_{mag,c} = 2.4$ J kg^{-1}K^{-1} are 6% greater and 30% smaller, respectively, than the average ΔS_{mag} of all the polycrystalline samples reported in Table 1 ($\Delta S_{mag,avg} = 3.4$ J kg^{-1}K^{-1} at $\mu_0 H = 2$ T)

Table 2
Magnetocrystalline anisotropy of $AlFe_2B_2$ calculated using different methods and with experimental and optimized structures.

Method	K (exp. structure)		K (opt. structure)	
	meV/f.u.	MJm^{-3}	meV/f.u.	MJm^{-3}
VASP-GGA	0.420	1.46	0.373	1.30
FP-GGA	0.425	1.47	0.382	1.34
FP-LDA	0.237	0.82	0.201	0.72

Note: Experimental value of K obtained for the crystallites is 0.9 ± 0.1 MJm^{-3}.

Table 3
Summary of magnetic properties of $AlFe_2B_2$ alloys with relevant references.

Synthesis Method	M_s (μ_B per Fe atom)	Curie temperature (K)	ΔS ($Jkg^{-1}K^{-1}$) 2T/5 T	Ref
Arc-melting[a]	1.15	282	4.4/7.3	[25]
Arc-melting[a]	0.95	320	–	[30]
Arc-melting[a]	1	285	1.3[b]/4.5	[31]
Arc-melting[a]	1.15	302	–	[24]
Ga-flux	1.03	307	4.1/7.7	[25]
Spark plasma sintered	–	274	3.1/6.4	[23]
Melt spinning	1.32	303	3.4/7.2	[27]
Suction cast/ annealed	1.18	284	2.8/-	[43]
Arc-melting	1.12[c]	285	2.4 ($\mu_0H \parallel$ c-axis)[c] 3.6 ($\mu_0H \parallel$ a-axis)[c]	This work

[a] Sample was purified by etching in HCl acid.
[b] ΔS measured at 1 T.
[c] The estimated error of the calculated values of M_s and ΔS is approx. ~10%.

The aligned $AlFe_2B_2$ crystallites exhibit a large room temperature rotating magnetocaloric effect near room temperature corresponding to $\Delta S_{rot,max} = 1.3\,J\,kg^{-1}K^{-1}$ at 285 K upon rotation between the *a* and *c*-axes in an applied magnetic field of 2 T, Fig. 6. In the magnetic field range 0.5 T–2 T, $\Delta S_{rot,max}$ increases with increase in applied magnetic field (Fig. 7). The $\Delta S_{rot,\ max}$ values obtained using Equation [3] are comparable to the difference between $\Delta S_{max,a}$ and $\Delta S_{max,c}$, indicating that the anisotropic character of the MCE is due to the anisotropy energy of the system alone. The field dependence of the anisotropy factor η, shown in Fig. 7(b), indicates a dramatic exponential decrease of η from *1* to *0.50* with increase in applied magnetic field from 0 to 1 T; subsequently η decreases from *0.50 to 0.28* as magnetic field is further increased to 2 T. It is therefore surmised that magnetocrystalline anisotropy energy influences the MCE of $AlFe_2B_2$ more significantly at low applied magnetic fields, particularly below 1 T.

The results obtained in this work have important relevance for magnetic refrigeration technology: magnetic cooling devices utilizing small magnetic fields (in the range, 1–2 T) should incorporate anisotropic, textured magnetocaloric materials, such as $AlFe_2B_2$, to make efficient use of the magnetic field energy. In addition to the results reported here on $AlFe_2B_2$, a large rotating magnetocaloric effect at room temperature has been reported for $NdCo_5$ single crystals (ΔS_{rot} (1.3 T) = 1.9 $J\,kg^{-1}K^{-1}$ at 280 K) and for an aligned polycrystalline alloy of $NdCo_4Al$ (ΔS_{rot} (1 T) = 1.9 $J\,kg^{-1}K^{-1}$ at 295 K) [21,22]. Finally, it is tentatively conjectured that the anisotropic growth habit of the $AlFe_2B_2$ crystallites, shown in Fig. 2(c), holds promise for magnetic refrigerators utilizing active magnetic regeneration (AMR) technology where the anisotropic working material may be shaped as periodic walls or channel structures for accelerating the heat transfer between the solid refrigerant and the pumped heat exchange fluid, while minimizing the pressure head on the fluid. At the current time, no information is available in the $AlFe_2B_2$ literature regarding the thermal properties of this compound. Future work aimed at investigation of the possible anisotropic character of the heat transfer properties of $AlFe_2B_2$ is planned and it is anticipated that this data will be valuable for complete assessment of the magnetocaloric potential of this materials system for applications in the power and energy sector.

5. Conclusions and outlook

An anisotropic magnetocaloric response of the intermetallic boride $AlFe_2B_2$ is confirmed through measurement of the response along the orthorhombic axes of single $AlFe_2B_2$ crystallites. In agreement with computational calculations, magnetic measurements indicate that within the (*ac*) plane, the crystallographic *a*- and *c*-axis is the easy and hard direction of magnetization, respectively, and the magnetocrystalline anisotropy in the (*ac*) plane is determined to be K~0.9 MJ/m^3 at 50 K. Accompanying magnetic entropy curves reveal large differences in magnetic entropy change ΔS_{mag} measured by applying the magnetic field along the *a*- and *c*-axis ($\Delta S_{max,a} = 3.6\,J\,kg^{-1}K^{-1}$ and $\Delta S_{max,c} = 2.4\,J\,kg^{-1}K^{-1}$ at $\mu_0 H = 2$ T), with a significant rotating magnetic entropy change near room temperature (1.3 $J\,kg^{-1}K^{-1}$ at $\mu_0 H_{app} = 2$ T). The morphology of the etched crystallites consists of crystallographically-oriented laminates of submicron thickness – a feature that holds promise for facile heat exchange between the regeneration fluid and the working material in an AMR refrigeration device. It is however critical to realize that the layered microstructure of the crystallites is not intrinsic in character. Instead, it is an artifact formed to preferential acid etching of the arc-melted precursor alloy along the anisotropic growth habit. It is construed that the efficiency of a prospective rotary magnetic cooling device using $AlFe_2B_2$, or another anisotropic compound, as the working material can be maximized by aligning pulverized powders into a porous compact. It is contemplated that the heat transfer characteristics of such a sample might be improved by addition of a small amount of a thermally conducting element (such as Cu) to facilitate formation of thermally conducting grain boundaries. Overall, this study provides insight of both fundamental and applied relevance concerning pathways for maximizing the magnetocaloric potential of $AlFe_2B_2$ for thermal management applications such as magnetic cooling and energy harvesting.

Funding Acknowledgement

We thank B. Jensen for useful discussions and S. Thimmaiah for help with sample characterization using x-ray diffraction. This work was conducted at Northeastern University and Ames Laboratory under the auspices of the U.S. Department of Energy (DOE), Advanced Research Projects Agency – Energy (DE-AR00000754). Ames Laboratory is operated for the U.S. Department of Energy by Iowa State University under Contract No. DE-AC02-07CH11358.

References

[1] V. Franco, J.S. Blázquez, B. Ingale, a. Conde, The magnetocaloric effect and magnetic refrigeration near room temperature: materials and models, Annu. Rev. Mater. Res. 42 (1) (2012) 305–342.
[2] C. Zimm, A. Jastrab, A. Sternberg, V.K. Pecharsky, K.A. Gschneidner Jr., M. Osborne, I. Anderson, Description and performance of a near-room temperature magnetic refrigerator, Adv. Cryog. Eng. 43 (1998) 1759.
[3] K.A. Gschneidner, V.K. Pecharsky, Magnetocaloric materials, Annu. Rev. Mater. Res. 30 (2000) 387–429.
[4] R. Barua, I. McDonald, F. Jiménez-Villacorta, D. Heiman, L. Lewis, Multivariable tuning of the magnetostructural response of a Ni-modified FeRh compound, J. Alloy. Comp. 689 (2016) 1044–1050.
[5] E. Brück, O. Tegus, D.T. Cam Thanh, N.T. Trung, K.H.J. Buschow, A review on Mn based materials for magnetic refrigeration: structure and properties, Int. J. Refrig. 31 (2008) 763–770.
[6] D.T. Cam Thanh, E. Brück, O. Tegus, J.C.P. Klaasse, T.J. Gortenmulder, K.H.J. Buschow, Magnetocaloric effect in MnFe (P, Si, Ge) compounds, J. Appl. Phys. 99 (8) (2009), 08Q107.

[7] Y. Koshkid'ko, S. Pandey, A. Quetz, A. Aryal, I. Dubenko, J. Cwik, E. Dilmieva, A. Granovsky, E. Lähderanta, A. Zhukov, S. Stadler, Inverse magnetocaloric effects in metamagnetic Ni-Mn-In-based alloys in high magnetic fields, J. Alloy. Comp. 695 (2017) 3348–3352.

[8] Y. Koshkid'ko, S. Pandey, A. Quetz, A. Aryal, I. Dubenko, J. Cwik, E. Dilmieva, A. Granovsky, E. Lähderanta, S. Stadler, N. Ali, Kinetic effects in the magnetic & magnetocaloric properties of metamagnetic $Ni_{50}Mn_{35}In_{14.25}B_{0.75}$, J. Magn. Magn. Mater. (2017). In Press.

[9] J. Lyubina, O. Gutfleisch, M.D. Kuz'min, M. Richter, La (Fe, Si) 13-based magnetic refrigerants obtained by novel processing routes, J. Magn. Magn Mater. 321 (21) (2009) 3571–3577.

[10] J. Liu, J.D. Moore, K.P. Skokov, M. Krautz, K. Löwe, A. Barcza, O. Gutfleisch, Exploring La (Fe, Si)13-based magnetic refrigerants towards application, Script. Mater. 67 (6) (2013) 584–589.

[11] M. Balli, S. Jandl, P. Fournier, A. Kedous-Lebouc, Advanced materials for magnetic cooling: fundamentals and practical aspects, Appl. Phys. Rev. 4 (2017) 021305.

[12] W. Jeitschko, The crystal structure of Fe_2AlB_2, Acta Crystal. 25 (1) (1969) 163.

[13] N.A. de Oliveira, P.J. von Ranke, Theoretical aspects of the magnetocaloric effect, Phys. Rep. 489 (4) (2010) 89–159.

[14] X. Bohigas, J. Tejada, F. Torres, J.I. Arnaudas, E. Joven, A. del Moral, Magnetocaloric effect in random magnetic anisotropy materials, Appl. Phys. Lett. 81 (13) (2002) 2427–2429.

[15] H. Tang, A.O. Pecharsky, D.L. Schlagel, T.A. Lograsso, V.K. Pecharsky, K.A. Gschneidner, Magnetic field induced phase transitions in $Gd_5(Si_{1.95}Ge_{2.05})$ single crystal and the anisotropic magnetocaloric effect, J. Appl. Phys. 93 (10) (2003) 8298–8300.

[16] F. Bitter, Magnetization and the magneto-caloric effect, Phys. Rev. 38 (3) (1931) 528.

[17] S.V. Vonsovsky, M.I. Katsnelson, Evolution of the concepts about the role of many-particle effects in transition metals, their alloys and compounds, Phys. B Condens. Matter 159 (1) (1989) 61–65.

[18] N.S. Akulov, L.W. Kirensky, J. Phys. 3 (1940) 31.

[19] M. Balli, B. Roberge, P. Fournier, S. Jandl, Review of the magnetocaloric effect in $RMnO_3$ and RMn_2O_5 multiferroic crystals, Crystals 7 (2) (2017) 44.

[20] S.A. Nikitin, K.P. Skokov, Y.S. Koshkidko, Y.G. Pastushenkov, T.I. Ivanova, Giant rotating magnetocaloric effect in the region of spin-reorientation transition in the $NdCo_5$ single crystal, Phys. Rev. Lett. 105 (2010) 137205.

[21] H. Zhang, Y. Li, E. Liu, Y. Ke, J. Jin, Y. Long, B. Shen, Giant rotating magnetocaloric effect induced by highly texturing in polycrystalline DyNiSi compound, Sci. Rep. 5 (2015) 11929.

[22] Y. Hu, Q.B. Hu, C.C. Wang, Q.Q. Cao, W.L. Gao, D.H. Wangand, Y.W. Du, Large room-temperature rotating magnetocaloric effect in NdCo 4 Al polycrystalline alloy, Solid State Commun. 250 (2017) 45–48.

[23] S. Hirt, F. Yuan, Y. Mozharivskyj, H. Hillebrecht, $AlFe_{2-x}Co_xB_2$ (x= 0–0.30): TC tuning through Co substitution for a promising magnetocaloric material realized by spark plasma sintering, Inorg. Chem. 55 (19) (2016) 9677–9684.

[24] P. Chai, S. a. Stoian, X. Tan, P.A. Dube, M. Shatruk, Investigation of magnetic properties and electronic structure of layered-structure borides AlT_2B_2 (T=Fe, Mn, Cr) and $AlFe_{2-x}Mn_xB_2$, J. Solid State Chem. 222 (2015) 52.

[25] X. Tan, P. Chai, C.M. Thompson, M. Shatruk, Magnetocaloric effect in AlFe2B2: toward magnetic refrigerants from earth-abundant elements, J. Am. Chem. 135 (2013) 9553–9557.

[26] Q. Du, G. Chen, W. Yang, Z. Song, M. Hua, H. Du, C. Wang, S. Liu, J. Han, Y. Zhang, J. Yang, Magnetic properties of $AlFe_2B_2$ and $CeMn_2Si_2$ synthesized by melt spinning of stoichiometric compositions, Jap. J. Appl. Phys. 54 (2015) 053003.

[27] Q. Du, G. Chen, W. Yang, J. Wei, M. Hua, H. Du, C. Wang, S. Liu, J. Han, Y. Zhang, J. Yang, Magnetic frustration and magnetocaloric effect in $AlFe_{2-x}Mn_xB_2$ (x = 0–0.5) ribbons, J. Phys. D Appl. Phys. 48 (2015) 335001.

[28] L.H. Lewis, R. Barua, B. Lejeune, Developing magnetofunctionality: coupled structural and magnetic phase transition in $AlFe_2B_2$, J. Alloy. Comp. 650 (2015) 482–487.

[29] M. Ade, H. Hillebrecht, Ternary borides Cr_2AlB_2, Cr_3AlB_4, and Cr_4AlB_6: the first members of the series $(CrB_2)_nCrAl$ with n = 1, 2, 3 and a unifying concept for ternary borides as MAB-phases, Inorg. Chem. 54 (13) (2015) 6122–6135.

[30] M. ElMassalami, D.S. Oliveira, H. Takeya, On the ferromangetism of $AlFe_2B_2$, J. Magn. Magn Mater. 323 (2011) 2133.

[31] J. Cedervall, M.S. Andersson, T. Sarkar, E.K. DelczegCzirjak, L. Bergqvist, T.C. Hansen, P. Beran, P. Nordblad, M. Sahlberg, Magnetic structure of the magnetocaloric compound $AlFe_2B_2$, J. Alloy. Comp. 664 (2016) 784–791.

[32] X.Q. Zheng, B.-G. Shen, Q. Du, G. Chen, W. Yang, Z. Song, M. Hua, H. Du, C. Wang, S. Liu, J. Han, Y. Zhang, J. Yang, Magnetic properties of $AlFe_2B_2$ and $CeMn_2Si_2$ synthesized by melt spinning of stoichiometric compositions, Jpn. J. Appl. Phys. 54 (2015).

[33] T. Ali, M.N. Khan, E. Ahmed, A. Ali, Phase analysis of $AlFe_2B_2$ by synchrotron X-ray diffraction, magnetic and Mössbauer studies, Prog. Nat. Sci.: Mater. Int. 27 (2) (2017) 251–256.

[34] L. Ke, B.N. Harmon, M.J. Kramer, Electronic structure and magnetic properties in T_2AlB_2 (T= Fe, Mn, Cr, Co, and Ni) and their alloys, Phys. Rev. B 95 (10) (2017) 104427.

[35] Cullity, Magnetic Materials, third ed., John Wiley and Sons, 1996.

[36] M. Fries, K.P. Skokov, D.Y. Karpenkov, V. Franco, S. Ener, O. Gutfleisch, The influence of magnetocrystalline anisotropy on the magnetocaloric effect: a case study on Co_2B, Appl. Phys. Lett. 109 (23) (2016) 232406.

[37] M. Methfessel, M. van Schilfgaarde, R.A. Casali, in: H. Dreysse (Ed.), Electronic Structure and Physical Properties of Solids: the Uses of the LMTO Method, vol. 535, Springer-Verlag, Berlin, 2000 of Lecture Notes in Physics.

[38] J.P. Perdew, K. Burke, M. Ernzerhof, Phys. Rev. Lett. 77 (1996) 3865.

[39] U. von Barth, L. Hedin, J. Phys. C Solid State Phys. 5 (1972) 1629.

[40] K. Cenzual, L.M. Gelato, M. Penzo, E. Parthé, Inorganic structure types with revised space groups. I, Acta Crystal. Sec. B: Struct. Sci. 47 (4) (1991) 433–439.

[41] G. Kresse, J. Furthmüller, Efficient iterative schemes for ab initio total-energy calculations using a plane-wave basis set, Phys. Rev. B 54 (16) (1996) 11169.

[42] J. Lu, S. Kota, M.W. Barsoum, L. Hultman, Atomic structure and lattice defects in nanolaminated ternary transition metal borides, Mat. Res. Lett. 5 (2016) 235–241.

[43] E. M. Levin, B. A. Jensen, R. Barua, B. Lejeune, A. Howard, R. W. McCallum, M. J. Kramer and L. H. Lewis, "Effects of Al content and annealing on the phases formation, lattice parameters, and magnetization of AlxFe2B2 (x = 1.0, 1.1, 1.2) alloys", Phys. Rev. Mater. (Accepted, In Press)